Neutron diffraction study of long-range interactions in gaseous krypton

1999 J. Phys.: Condens. Matter 11 3091

(http://iopscience.iop.org/0953-8984/11/15/014)

J. Phys.: Condens. Matter **11** (1999) 3091–3104. Printed in the UK PII: S0953-8984(99)98033-5

Neutron diffraction study of long-range interactions in gaseous krypton

Chris J Benmore†*, Ferdinando Formisano‡§#, Renato Magli§‖, Ubaldo Bafile§¶, Peter Verkerk+, Peter A Egelstaff† and Fabrizio Barocchi‡§

† Physics Department, University of Guelph, Ontario, Canada N1G 2W1
‡ Dipartimento di Fisica, Università di Firenze, l.go E. Fermi 2, I-50125 Firenze, Italy
§ Istituto Nazionale di Fisica della Materia, Sez. di Firenze, l.go E. Fermi 2, I-50125 Firenze, Italy
‖ Dipartimento di Energetica 'S Stecco', Università di Firenze, v. di S Marta 3, I-50139 Firenze, Italy
¶ Istituto di Elettronica Quantistica, Consiglio Nazionale delle Ricerche, v. Panciatichi 56/30, I-50127 Firenze, Italy
+ Interfacultair Reactor Instituut, Technische Universiteit Delft, Mekelweg 15, 2629 JB Delft, The Netherlands

Received 30 September 1998, in final form 11 December 1998

Abstract. The low-Q part ($0.47 < Q\ (\mathrm{nm}^{-1}) < 4.15$) of the static structure factor $S(Q)$ of ^{86}Kr has been derived at five low densities and room temperature by a small-angle neutron diffraction measurement and a careful treatment of experimental corrections. From the data the small-Q dependence of the Fourier transform $c(Q)$ of the direct correlation function $c(r)$ has been obtained and has allowed the first accurate experimental determination of the long-range three-body Axilrod–Teller potential strength in a classical fluid.

1. Introduction

The interatomic structure factor of a fluid contains useful information about both the short- and long-range parts of the pair potential and also about higher-order potentials. The short-range part is better understood and more accessible than the long-range part. But several theoretical papers have emphasized the importance of experimental studies of the long-ranged terms. For example Enderby *et al* [1] consider the dependence of the structure factor $S(Q)$ (related to the Fourier transform of the pair correlation function) on the argument Q, and for low values of Q they write:

$$S(Q) = S(0) + S_2 Q^2 + S_3 Q^3 + \cdots \tag{1}$$

with

$$S_3 = \frac{\pi^2 \beta n \{S(0)\}^2 B}{12} \tag{2}$$

where $\beta = 1/k_\mathrm{B}T$, T is the temperature, k_B is the Boltzmann constant, $S(0) = n\chi_T/\beta$, n is the number density, χ_T is the isothermal compressibility, and the van der Waals term B is the coefficient of the long-ranged r^{-6} term in the pair interaction (see equation (10)). This r^{-6}

* Present address: ISIS Division, Rutherford Appleton Laboratory, Chilton, Didcot, Oxfordshire OX11 0QX, UK.
# Present address: Laboratoire Léon Brillouin, CEA Saclay, 91191 Gif-sur-Yvette Cédex, France. LLB is a Laboratoire Commun CEA-CNRS.

0953-8984/99/153091+14$19.50

interaction between two electronic ground state atoms is determined by the London dispersion energy. For S_2 there is no known analytical expression in terms of the potential parameters. Casanova *et al* [2] considered the addition of the Axilrod–Teller (AT) three-body force [3] in low-density gases, and showed that an additional density dependent term should be added to the Q^3 coefficient (2). In a later paper Matthai and March [4] used (1) to interpret an *extrapolation* of the experimental data on liquid argon to very small values of Q. This work illustrated the experimental problems in isolating the Q^3 term, namely that very accurate data would be necessary at very small values of Q, so that higher-order terms in (1) would be negligible.

A more detailed analysis of the Q dependence, including numerical predictions, was presented by Reatto and Tau [5]. In addition to discussing the classical behaviour of the Q^3 term, they considered retardation effects related to the finite velocity of propagation of the electromagnetic field. This effect alters the Q^3 behaviour to $Q^4 \ln(Q)$ at very low values of Q, thus defining a lower limit for the Q range where the Q^3 term can be detected. They show, in fact, that, by measuring the Fourier transform $c(Q)$ of the direct correlation function (see equation (6)) in the range $0.5 < Q\ (\mathrm{nm}^{-1}) < 3.5$ at intermediate density, one should be able to extract the Q^3 term, and that, for this purpose, the use of $c(Q)$ is preferable to that of $S(Q)$. Experimental determination of the coefficient of the Q^3 term would be of fundamental importance because of the direct and simple relationship with the long-range behaviour of the interatomic interaction. Magli *et al* [6] applied for the first time the low-Q expansion for the experimental determination of the coefficient B of the London dispersion term in argon, but the experimental accuracy did not allow for a determination of the strength of the AT-triple dipole interaction.

In addition, the density dependence of $S(Q)$ at constant Q is interesting, especially the relationships involving both pair and many-body forces, which has been discussed in several papers [7–9]. For example Tau *et al* [9] reviewed recent data on krypton and calculated the contribution of various models for the pair and three-body interactions to the coefficients of the density expansions of $S(Q)$ and $c(Q)$. They find that the dependence of $c(Q)$ on the detailed shape of the pair potential is mainly contained in the constant term (i.e. the zero-density limit), but this is not the case for $S(Q)$. So, also here it is preferable to use $c(Q)$ instead of $S(Q)$.

In this paper we try to meet some of these challenges, by experiments on krypton gas. Our method is to improve the quality of the data by employing the isotope ^{86}Kr and also to use a modern small-angle diffractometer in order to extend to lower values the range of Q investigated in the earlier extensive study by Teitsma and Egelstaff [7]. They covered a wide range of densities of natural krypton at room temperature and used a conventional neutron diffractometer with $2 < Q\ (\mathrm{nm})^{-1} < 40$. The general behaviour of the pair potential could be extracted and the contribution of the three-body terms examined. Therefore, their data form a convenient starting point for our investigation, in which several densities, overlapping those of [7], have been studied.

In a previous paper [10] we have briefly described the results of our experiment, with the determination of the van der Waals coefficient B and the AT interaction strength. The former turns out to be in agreement with previous estimates, and in this paper we concentrate on a refined determination of the latter, by including in the analysis the results of two more thermodynamic states and exploiting more efficiently the physical information contained in the full measured Q range.

Section 2 reviews the theory, while section 3 covers the experimental method and section 4 the data analysis. The results are shown in section 5 and we summarize our conclusions in section 6. Some details of the data correction are illustrated in an appendix.

2. Theoretical summary

In the theory of simple monatomic fluids, the most relevant quantity for the description of the microscopic structural properties is the static structure factor $S(Q)$, which is related to the pair correlation function $g(r)$ by

$$S(Q) = 1 + n \int \mathrm{d}\boldsymbol{r} \exp(-\mathrm{i}\boldsymbol{Q}\cdot\boldsymbol{r})[g(r) - 1]. \tag{3}$$

It is useful to introduce also the direct correlation function $c(r)$, defined via the Ornstein–Zernike relation (with $h(r) = g(r) - 1$)

$$h(r) = c(r) + n \int \mathrm{d}\boldsymbol{r}'\, c(r')h(|\boldsymbol{r} - \boldsymbol{r}'|) \tag{4}$$

and its Fourier transform

$$c(Q) = \int \mathrm{d}\boldsymbol{r} \exp(-\mathrm{i}\boldsymbol{Q}\cdot\boldsymbol{r})c(r). \tag{5}$$

From (3)–(5) $c(Q)$ can be expressed in terms of the experimentally accessible quantity $S(Q)$ as

$$c(Q) = \frac{1}{n}\left(1 - \frac{1}{S(Q)}\right). \tag{6}$$

For classical systems of N atoms, $g(r)$ and $c(r)$ are functionals of the interatomic interaction potential energy $U(\boldsymbol{r}_1, \ldots, \boldsymbol{r}_N)$, for which a cluster expansion will be assumed to be valid at densities below the critical one:

$$U(\boldsymbol{r}_1, \ldots, \boldsymbol{r}_N) = \sum_{i<j} u_2(r_{ij}) + \sum_{i<j<k} u_3(\boldsymbol{r}_i, \boldsymbol{r}_j, \boldsymbol{r}_k) + \cdots. \tag{7}$$

Here $\boldsymbol{r}_i$ is the position of the ith atom, $r_{ij} = |\boldsymbol{r}_i - \boldsymbol{r}_j|$, and u_2 and u_3 are the pair and triplet irreducible interaction potentials, respectively.

Among the various properties of the interaction potential which can be probed by measuring $S(Q)$, one of particular interest here is the asymptotic behaviour at large distances. In fact, if only the pair and triplet terms are retained in (7) by neglecting many-body forces beyond the triplet level, it can be demonstrated [2, 5] that

$$c(r) \underset{r\to\infty}{\sim} -\beta u_2(r) + D(r) \tag{8}$$

where $D(r)$ is the so-called dressed three-particle vertex

$$D(r_{12}) = n \int \mathrm{d}\boldsymbol{r}_3\, g(r_{13})g(r_{23})\{\exp[-\beta u_3(\boldsymbol{r}_1, \boldsymbol{r}_2, \boldsymbol{r}_3)] - 1\}. \tag{9}$$

Equation (8) shows that $c(r)$, and consequently $c(Q)$, directly reflect the properties of the interatomic interaction at large distances. For an insulating fluid in its ground state the dispersion term dominates the pair potential at large interatomic distances:

$$u_2(r) \underset{r\to\infty}{\sim} -Br^{-6} \tag{10}$$

and, if the triple-dipole AT expression

$$u_3(\boldsymbol{r}_1, \boldsymbol{r}_2, \boldsymbol{r}_3) = \nu \frac{1 + 3\cos\theta_1 \cos\theta_2 \cos\theta_3}{(r_{12}r_{13}r_{23})^3} \tag{11}$$

is assumed to represent the irreducible three-body potential, where ν is the amplitude and θ_1, θ_2, θ_3 and r_{12}, r_{13}, r_{23} are the angles and side lengths of the triangle formed by three atoms, one has [2, 5]

$$D(r) \underset{r\to\infty}{\sim} -\frac{8\pi}{3}\beta n \nu r^{-6}. \tag{12}$$

Because of (8), (10) and (12) $c(r)$ decays asymptotically to zero as r^{-6}, and by means of asymptotic Fourier analysis it is possible to demonstrate [1, 5] that this implies that $c(Q)$ can be expanded at low Q as

$$c(Q) = c(0) + \gamma_2 Q^2 + \gamma_3 |Q|^3 + \gamma_4 Q^4 + \cdots \tag{13}$$

and in particular it contains a $|Q|^3$ term, non-analytical at $Q = 0$, with a coefficient γ_3 directly proportional to the amplitude of the r^{-6} tail of $c(r)$ and given by

$$\gamma_3 = \frac{\pi^2 \beta}{12}\left(B - \frac{8\pi}{3} n \nu\right). \tag{14}$$

Therefore, the extraction of the cubic term in the small-Q behaviour of $c(Q)$ for at least two different densities provides a direct measurement of the van der Waals parameter B and the AT amplitude ν. We point out that in general both $c(0)$ and γ_2 depend on u_2 and u_3, but no analytical expressions in terms of B and ν exist. For this reason we have used numerical methods [10] to exploit these relationships, and we shall discuss such results in section 5.

Theoretical calculations performed by means of the modified hyper-netted chain (MHNC) integral equations, including the AT three-body term [5], have indicated that the suitable Q-range for the extraction of γ_3 is $0.5 < Q\ (\mathrm{nm}^{-1}) < 3.5$. This is an important result because that is the Q range which is typically accessible in a small-angle neutron diffraction experiment, so that the feasibility of such a measurement of γ_3 mainly depends on the magnitude of the effect compared to the other terms in (13) and to the overall accuracy that can be obtained in the measurement of $c(Q)$.

As already mentioned in the introduction, an expansion similar to (13) can be written for the structure factor (see (1)). However, it has been clearly shown [5] that there are two advantages in using the Q expansion of $c(Q)$ instead of $S(Q)$: first, γ_3 has the much simpler dependence on the thermodynamic coordinates shown in (14), while $S_3 = n[S(0)]^2\gamma_3$ is state dependent also through the isothermal compressibility χ_T (see equation (2)); secondly, the range of Q where the Q^4 term is negligible is much narrower in the expansion of $S(Q)$ thus making it more difficult to extract the cubic part.

For the purposes of the present work it is particularly useful to consider the virial (i.e. density) expansion of $c(Q)$ which is written at low density as [9]

$$c(Q) = c_0(Q) + n c_1(Q) + \mathrm{O}(n^2) \tag{15}$$

where the zero-order term depends on u_2 simply as

$$c_0(Q) = \int \mathrm{d}\boldsymbol{r} \exp(-\mathrm{i}\boldsymbol{Q}\cdot\boldsymbol{r})[\exp(-\beta u_2(r)) - 1]. \tag{16}$$

The next term in (15) describes the effect of a third particle and is composed of two parts which depend, respectively, on u_2 only and on both u_2 and u_3. We will denote it as

$$c_1(Q) = c_1^{(2)}(Q) + c_1^{(3)}(Q) \tag{17}$$

where

$$c_1^{(2)} Q = \int \mathrm{d}\boldsymbol{r}_{12}\, \mathrm{d}\boldsymbol{r}_{13} \exp(-\mathrm{i}\boldsymbol{Q}\cdot\boldsymbol{r}_{12}) f_{12} f_{13} f_{23} \tag{18}$$

$$c_1^{(3)}(Q) = \int \mathrm{d}\boldsymbol{r}_{12}\, \mathrm{d}\boldsymbol{r}_{13} \exp(-\mathrm{i}\boldsymbol{Q}\cdot\boldsymbol{r}_{12})(1 + f_{12})(1 + f_{13})(1 + f_{23}) f_{123}. \tag{19}$$

In the last two equations $f_{ij} = \exp[-\beta u_2(r_{ij})] - 1$ is the Mayer function, and $f_{123} = \exp[-\beta u_3(\boldsymbol{r}_1, \boldsymbol{r}_2, \boldsymbol{r}_3)] - 1$. We shall show that in the present experiment the sample densities were low enough for terms of order n^2 and higher to be negligible in (15).

3. Experiment

The measurements were performed on the small-angle diffractometer PAXE at the Orphée reactor of the Laboratoire Léon Brillouin, Saclay. The cross section of the incident neutron beam was defined by a 9 mm circular diaphragm placed in front of the sample container, and the wavelength λ was 0.40 ± 0.03 nm. The two-dimensional BF_3 detector, made of 64×64 cells each 1×1 cm^2, was placed at 171.5 cm from the centre of the sample and rotated around the sample position by such an amount as to have the detector centre horizontally shifted by 16 cm with respect to the incident neutron beam. The detector cells were grouped together in rings of 1 cm width centred around the beam position, so that all cells in a ring correspond to the same scattering angle θ. This configuration allows one to probe a momentum transfer range $0.5 < Q\ (\mathrm{nm}^{-1}) < 4.3$, with a resolution $\Delta Q/Q \approx 10\%$. Due to the smooth monotonic behaviour versus Q of the diffraction spectra, the modest Q resolution does not affect the results presented below. Between the exit window of the sample cell (see below) and the 27 mm thick sapphire window at the entrance of the vacuum tank containing the detector was an air gap of 27 mm.

The sample cell, approved for use at pressures up to 800 bar, is made of stainless steel with single-crystal sapphire windows of 8 mm thickness for the incident beam and 15 mm for the outgoing neutrons. The inner distance between the two windows is 34.8 mm. In order to minimize the amount of ^{86}Kr required to fill the container during the measurements, the inner volume of the cell was designed to be of conical shape, internally clad with cadmium.

In order to reduce absorption and incoherent scattering we used a sample of the isotope ^{86}Kr. Its composition for Kr isotopes was 99.3% for ^{86}Kr and 0.7% for ^{84}Kr. A maximum contamination of 0.14 mol% nitrogen and 0.14 mol% hydrocarbon gases was declared by the manufacturer. The coherent scattering cross section $\sigma_c = 8.2 \pm 0.5$ b was measured previously by means of neutron interferometry on the same gas [11], while in a transmission experiment [11] no incoherent scattering could be detected within the experimental accuracy and we assume $\sigma_{\mathrm{inc}} = 0$. Moreover, we use $\sigma_{\mathrm{abs}} = 0.007 \pm 0.004$ b for $\lambda = 0.4$ nm [12].

Table 1. Pressure P, number density n, ratio of n to the critical number density $n_{\mathrm{cr}} = 6.53\ \mathrm{nm}^{-3}$ and thermodynamic value of $S(0)$ for each of the measurements. n and $S(0)$ are derived from the equation of state of [13]. Also the values S_0 at $Q = 0$ from the least squares fit to the experimental $S(Q)$ are given. The estimated uncertainties for n and $S(0)$ are 0.5%.

State	P (bar)	n (nm^{-3})	n/n_{cr}	$S(0)$	S_0
1	30.9 ± 0.1	0.804	0.123	1.141	1.135 ± 0.003
2	55.5 ± 0.2	1.522	0.233	1.270	1.257 ± 0.002
3	69.8 ± 0.3	1.984	0.303	1.352	1.330 ± 0.002
4	77.1 ± 0.3	2.231	0.342	1.394	1.346 ± 0.002
5	83.2 ± 0.3	2.431	0.372	1.423	1.390 ± 0.003

All measurements were made at room temperature ($T = 297.6 \pm 0.5$ K). The equation-of-state data of Jůza and Šifner [13] are used for determining the number densities and the isothermal compressibilities of the five investigated states of Kr, which are given in table 1 and will be referred to by the numbering shown in the first column. The slight differences between the present values and the ones reported in [10] are due to the fact that in this work the more recent data of [13] have been used. In order to apply all corrections and to obtain absolutely normalized data, additional measurements were made on the empty cell, empty beam, cadmium foil, 1.6 mm thick vanadium foil and methane at 2.30 bar ($n = 0.0562\ \mathrm{nm}^{-3}$). The main advantage of using CH_4 instead of V for normalization is that with CH_4 the same

container as for the krypton could be used, avoiding systematic errors due to geometrical effects or exchanging samples. However, an accurate model for the dynamic structure factor of CH_4 is required [14]. The V measurement was made without the cell and used for comparison. The beam time for the measurements on ^{86}Kr, V and CH_4 was adjusted to achieve a statistical error less than 0.5% in all experimental intensities. To monitor the stability of the experimental setup each measurement was split into several runs. Figure 1 gives the raw data for the various samples, in units of counts per cell per thousand monitor counts.

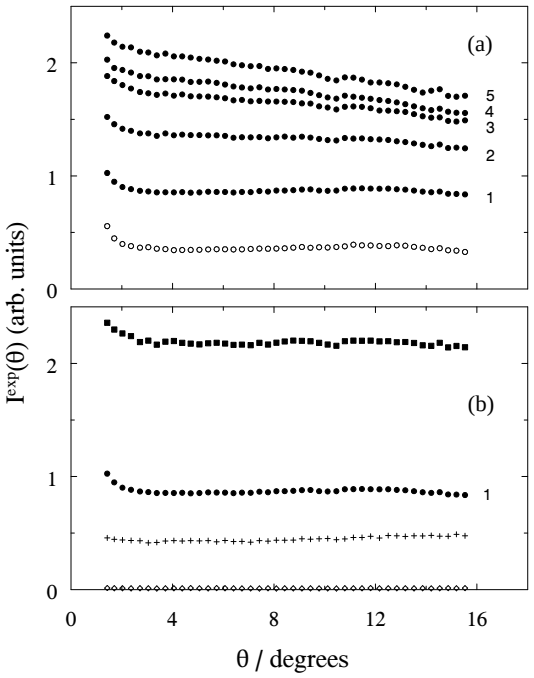

Figure 1. Experimental intensities I^{exp} for the various measurements. In (a): empty cell (open circles) and Kr at the various densities (full circles from 1 to 5). The lowest Kr density (full circles) is also shown for comparison in (b) together with cadmium (open diamonds), empty beam (crosses) and methane (squares). In all spectra error bars are smaller than the size of the symbols. The data are normalized to the number of detector cells at each θ and to thousand monitor counts.

4. Corrections and data reduction

The data recorded with a cadmium foil in place of the 9 mm diaphragm have a very low, almost constant intensity (see figure 1). After having subtracted this background, a ratio of the empty cell to the empty beam spectra of $\sim$0.81 for intermediate angles is obtained, whereas the empty cell transmission at $\theta = 0^\circ$ was calculated and measured to be higher than 0.9. This unexpected higher attenuation could be explained if one bears in mind that the cross section of sapphire rises at wavelengths shorter than 0.4 nm [15] and assuming that there is a 'halo' with an average wavelength less than 0.4 nm around the beam of 0.4 nm neutrons. It is worth mentioning that these halo neutrons are not present in the cadmium run, therefore they must be a component of the beam. Also, the halo extends over all angles seen by the detector, and at the largest angles it is restricted by the cadmium shielding in the sapphire cell. This would explain the 'droop' seen on the empty cell spectra at high angles, as the cadmium

lined cell would be collimating the halo. This effect is not seen when there is nothing in the beam. Further evidence of the spreading of the halo neutrons over the angles is obtained comparing the empty beam and the cadmium measurements which should be essentially the same, if the halo were not present. Drawing rays back from the detector suggests that the velocity selector might have transmitted a beam with an epithermal component (as well as 0.4 nm) and that component is scattered by the guides. This might confirm earlier observations [16].

Therefore, all spectra should be split into two parts: a 0.4 nm beam and the neutron halo part. However, in the appendix we show that, in the case of the present experiment, explicit correction for the halo leads to results for the fully corrected $c(Q)$ which, within our experimental errors, coincide well with the $c(Q)$ obtained by treating the background in the conventional way, i.e. as if it were due entirely to 0.4 nm neutrons. Therefore, we present here the results from the conventional correction procedure [17]. The details are given in the appendix.

After correcting for background, multiple scattering and self-shielding, and normalizing by means of the CH_4 measurement, the observed differential scattering cross section per atom is given by:

$$\left(\frac{\mathrm{d}\sigma}{\mathrm{d}\Omega}\right) = \left[\frac{\sigma_{\mathrm{inc}}}{4\pi} + \frac{\sigma_{\mathrm{c}}}{4\pi}S(Q)\right] + \frac{\sigma_{\mathrm{s}}}{4\pi}P(Q) \tag{20}$$

where in the present case $\sigma_{\mathrm{inc}} = 0$, and $P(Q)$ is the correction due to inelastic scattering including the wavelength dependent detector efficiency, calculated according to [18]. $P(Q)$ is less than 3% for all densities in the present case.

Because the bound atom cross section of hydrogen is about ten times greater than that of ^{86}Kr, it is necessary to consider the effect of possible hydrogen impurities carefully. The absolute magnitude of the scattering which would be produced by the maximum amount of hydrogeneous contaminants is within the error of the ^{86}Kr cross section. By assuming for the intensity scattered by these possible impurities a physically reasonable dependence on Q, we have also estimated that the differences which the presence of such impurities would introduce in the slope of the final $c(Q)$ would be less than the experimental errors.

The value of $S(Q)$ at $Q = 0$ is also obtained from *PVT* data and agrees well with the neutron data at all densities (maximum deviation less than 4%, average deviation 1.8%). In order to eliminate even these small differences a final renormalization of the measured $S(Q)$ was performed using the ratio $S(0)/S_0$, with $S(0)$ from PVT data and S_0 obtained from fitting the model function $S(Q) = S_0 + S_2Q^2 + S_3Q^3$ (see (1)) to the experimental data. This renormalization factor varied between 1.006 and 1.036 depending on the density. We note that, due to a new determination of densities and compressibilities, a slightly different renormalization is obtained for the present data compared to those reported in [10]. The renormalized $S(Q)$ values are shown in figure 2, where the data by Teitsma and Egelstaff [7] are also reported for comparison. The agreement between the two sets of data is very good, apart from the highest Q values at the two lowest densities, where a small systematic deviation seems to be present. The experimental $c(Q)$ values were derived using (6) and the measured structure factors, and are displayed in figure 3.

5. Results

A least-squares fit of (13) to the data for $c(Q)$ was performed at each density up to the Q^3 term. The fit does not improve significantly by including the term γ_4Q^4, therefore we deleted all terms of order 4 and higher. The fitted polynomials, also shown in figure 3, describe very

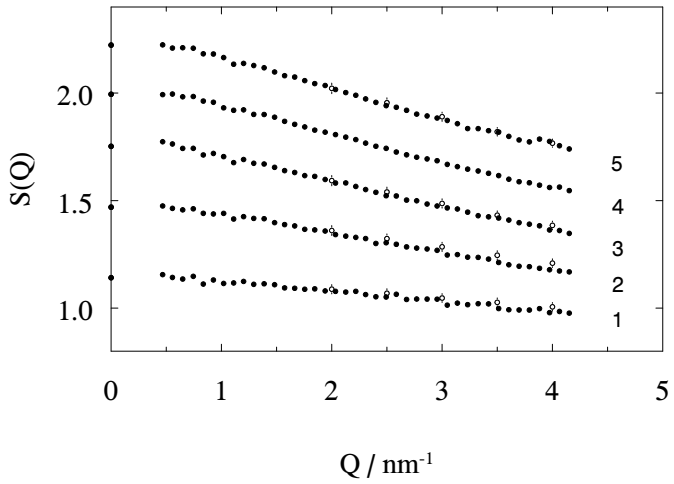

Figure 2. Experimental $S(Q)$ (dots) at the various densities. Data are shifted upwards by 0.2, 0.4, 0.6, 0.8 for states 2 to 5, respectively. The open circles are data from [7] at densities very close to those of the present experiment: from bottom to top, $n = 0.799$, 1.517, 1.964 and 2.425 nm^{-3} (the last three are shifted upwards by 0.2, 0.4 and 0.8, respectively). In all spectra of the present experiment error bars are smaller than the size of the symbols. The dots at $Q = 0$ are thermodynamic values [13].

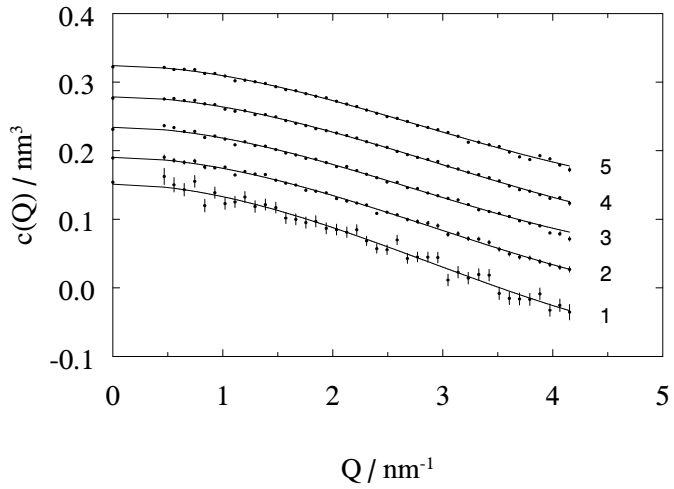

Figure 3. Experimental $c(Q)$ (dots with error bars) at the various densities. Data are shifted upwards by 0.05, 0.10, 0.15, 0.20 for states 2 to 5, respectively. The dots at $Q = 0$ are thermodynamic values [13]. The lines are least-squares fits of model (13) up to and including the Q^3 term.

well the Q dependence of $c(Q)$.

We note that, due to the smallness of the Q^3 term in (13), and of the density dependent contribution in (14) with respect to the constant one, the accuracy of the present data is not sufficient for the simultaneous determination of B and ν from (14). Such a determination, if possible, would be a direct measurement of these parameters, independent of any assumption

on the pair potential.

We have demonstrated in [10] that the experimental value of B that can be extracted from our data, i.e. $(13 \pm 1) \times 10^{-24}$ J nm^6, is in agreement with, although much less accurate than, previous semiempirical results for B, namely $(12.7 \pm 0.9) \times 10^{-24}$ J nm^6 [19], $(12.4 \pm 0.1) \times 10^{-24}$ J nm^6 [20] and $(12.2 \pm 0.1) \times 10^{-24}$ J nm^6 [21]. Therefore we will focus here on the experimental determination of ν.

In [10] it has also been shown that the γ_2 coefficient in the Q expansion (13) of $c(Q)$ is more sensitive to the three-body intensity ν than γ_3. It has to be noted that the coefficient $c(0)$, which is closely connected to thermodynamics through the compressibility equation, is also strongly affected by the three-body potential. However, since no known analytical expressions relate ν to $c(0)$ and γ_2, in [10] we were forced to apply a numerical analysis to find ν from γ_2. Here we present an alternative method which is based on the use of the virial expansion (15) of the full $c(Q)$. It can be shown that this procedure, which uses all the information on ν contained in the experimental $c(Q)$, further increases the sensitivity to ν with respect to the one adopted in [10].

We used (15) to evaluate $c_0(Q)$ and $c_1(Q)$ at all the Q values of the experiment. The experimental $c(Q)$ turns out to depend linearly on density, at fixed Q, in the whole investigated ranges of n and Q. The density dependence is shown in figure 4 for a few values of Q together with the straight lines obtained from a linear least-squares fit.

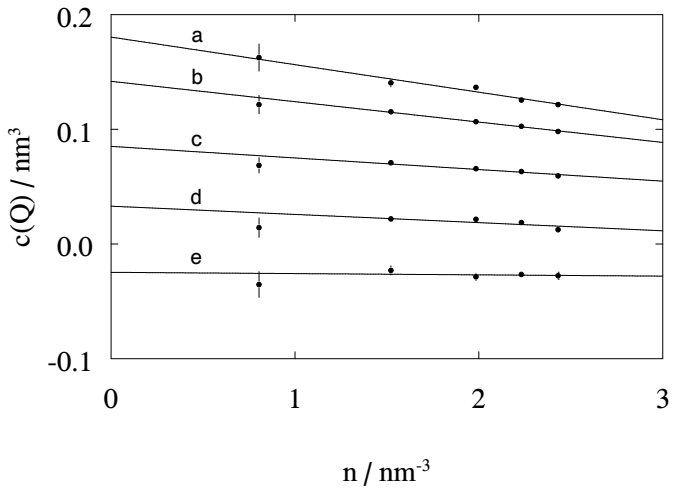

Figure 4. Density behaviour of $c(Q)$ at $Q = 0.47$, 1.39, 2.31, 3.23 and 4.15 nm^{-1} for curves (a) to (e), respectively: experimental points (dots with error bar) and best linear fits (solid lines).

The linearity of $c(Q)$ as a function of n allows us to compare the experimental data to calculated quantities by using (15)–(19) to compute $c(Q)$ for given potentials u_2 and u_3. We assume as a realistic model for u_2 the one given by Aziz and Slaman (AS) with $B = 12.5 \times 10^{-24}$ J nm^6 [22], while for u_3 we take the AT expression with an amplitude $\nu_0 = 2.22 \times 10^{-26}$ J nm^9 (that is, the average of three semiempirical determinations reported in the literature with uncertainties of the order of 1–2%, namely 2.23×10^{-26} J nm^9 [19, 20] and 2.20×10^{-26} J nm^9 [21]). The resulting curves for $c(Q)$ with and without the AT three-body interaction are shown in figure 5. The overall agreement with the measured data is good, especially if the AT potential is taken into account. A closer look reveals that the correspondence is best at the intermediate densities, while for the lowest and the highest ones

some discrepancy, with opposite signs in the two cases, arises at the larger Q values. Since these discrepancies are small but have a clear density dependence, they appear more evidently in the fitted parameters $c_0(Q)$ and $c_1(Q)$ of the virial expansion (15), which show a good agreement with the calculated ones for $Q < 2$ nm^{-1}, but deviate from them at larger Q-values. In particular, the experimental $c_0(Q)$ is lower and $c_1(Q)$ higher than the calculations, in such a way that these deviations compensate each other, at least partially, when the total $c(Q)$ is evaluated, which explains why no clear deviations are visible in figure 2 of [10] and in the present figure 5.

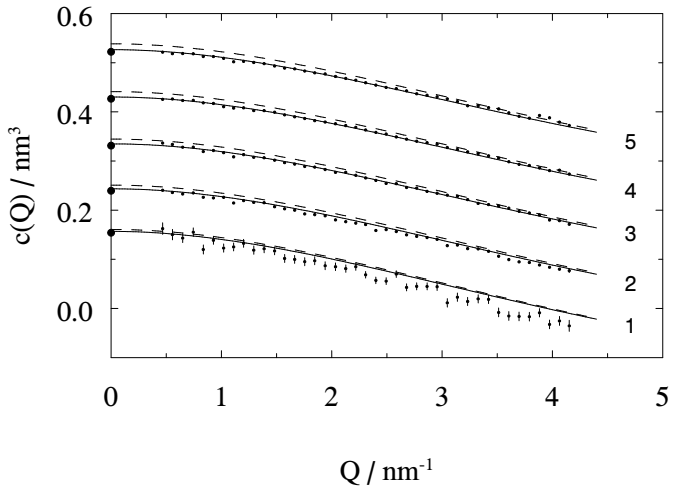

Figure 5. $c(Q)$ calculated from virial series (15) with two-body AS [22] and three-body AT [3] potential with $\nu = \nu_0 = 2.22 \times 10^{-26}$ J nm^9 (full lines) and without AT potential (dashed lines). For comparison the experimental data of figure 3 are shown again. Data are shifted upwards by 0.10, 0.20, 0.30, 0.40 for states 2 to 5, respectively. The dots at $Q = 0$ are thermodynamic values [13].

It is therefore more reliable to determine the three-body potential strength ν from the total $c(Q)$ rather than from its density expansion. The method is based on the assumption that the pair potential is accurately represented by the AS model and that the three-body interaction has the analytical form (11). In order to determine ν by this method, we first checked that the ratio $c_1^{(3)}(Q)/\nu$, calculated using (19), is independent of ν over the whole Q range of the present experiment. This appears indeed to be the case within 0.2% for $\nu < 3 \times 10^{-26}$ J nm^9 and allows us to determine ν as the value which gives the best agreement between experimental data and calculations of $c(Q)$, by varying ν and scaling $c_1^{(3)}(Q)$ proportionally. To this aim we have rewritten (15) as

$$c(Q) - c_0(Q) - nc_1^{(2)}(Q) = nc_1^{(3)}(Q, \nu = \nu_0)\frac{\nu}{\nu_0} \tag{21}$$

so that, using the experimental data for $c(Q)$, and the calculated $c_0(Q)$, $c_1^{(2)}(Q)$ and $c_1^{(3)}(Q, \nu = \nu_0)$, ν can be obtained by averaging the values determined at each density and each Q. We remark that the experimental information used in (21) is given by the total $c(Q)$, not the fitted density coefficients $c_0(Q)$ and $c_1(Q)$. Moreover, in order to minimize the effect of the slight discrepancy shown in figure 5 between the calculated and measured $c(Q)$, and to obtain a more reliable determination of ν, we have restricted the number of used experimental points to that region of the (Q, n) space where the data are fully compatible with the chosen potential models.

The selection of the Q points satisfying this condition has been achieved by minimizing, at each density and with respect to ν, the quantity

$$\chi^2(\nu) = \frac{1}{(N_Q - 1)} \sum_{i=1}^{N_Q} \frac{[c^{(3)}_{1,\mathrm{exp}}(Q_i) - c^{(3)}_{1,\mathrm{calc}}(Q_i, \nu)]^2}{s_i^2} \tag{22}$$

where $c^{(3)}_{1,\mathrm{exp}}(Q_i)$ is the left-hand side of (21), divided by the density, measured at $Q = Q_i$ with estimated standard deviation s_i, $c^{(3)}_{1,\mathrm{calc}}(Q_i, \nu)$ is the corresponding calculated quantity and N_Q is the number of points Q_i, numbered in order of increasing Q. The calculation of the minimum $\chi^2(\nu)$ has been performed at each density as a function of N_Q.

We have then applied (21) to the determination of ν using all points at the intermediate densities, the first 21 points at the lowest one, and the first 23 points at the highest one. The resulting weighted-averaged value is $\nu = (2.40 \pm 0.21) \times 10^{-26}$ J nm^9, in agreement with ν_0. We estimate that the systematic uncertainty associated with the chosen normalization procedure is 0.25×10^{-26} J nm^9. This new determination of ν is consistent with, but much more accurate than, the one reported in [10], because of the different way of analysing data and because in [10] only three densities out of the five measured had been considered. However, since $B \gg 8\pi\nu n/3$, this does not significantly change the result for B obtained in [10].

Figure 6 shows $c^{(3)}_{1,\mathrm{exp}}(Q)$ averaged over all the densities considered at each Q, together with $c^{(3)}_{1,\mathrm{calc}}(Q, \nu)$ calculated with both $\nu = \nu_0$ and the value of ν obtained above. It is interesting to look at the plot of $\chi^2(\nu)$ as a function of ν (figure 7), which clearly shows that the sensitivity to ν is enhanced at the higher densities, where the value of ν that minimizes χ^2 is very stable.

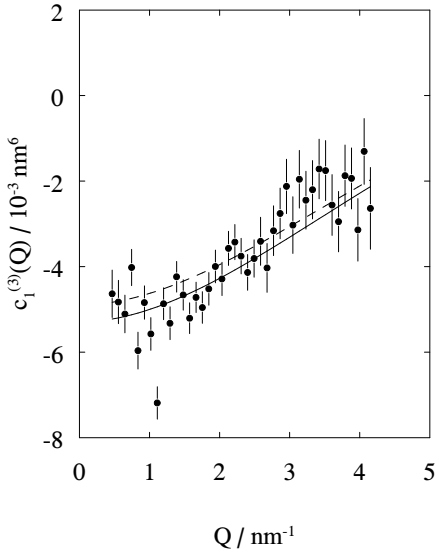

Figure 6. $c^{(3)}_{1,\mathrm{exp}}(Q)$ averaged over density as described in the text (dots with error bars) and $c^{(3)}_{1,\mathrm{calc}}(Q, \nu)$ calculated with $\nu = \nu_0$ (dashed line) and $\nu = 2.40 \times 10^{-26}$ J nm^9 (solid line).

6. Conclusions

The main result of this work consists in a new improved experimental determination of the Axilrod–Teller three-body strength ν for krypton. We have improved on our previous [10]

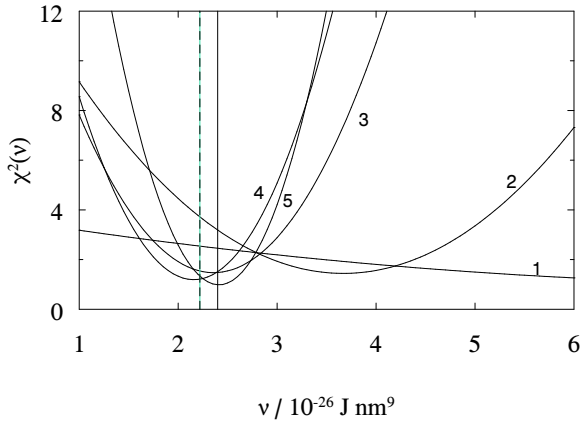

Figure 7. $\chi^2(\nu)$ as defined in (22) at the five experimental densities. The vertical lines correspond to ν_0 (dashed line) and to $\nu = 2.40 \times 10^{-26}$ J nm^9 (solid line).

result, obtaining $\nu = 2.40 \times 10^{-26}$ J nm^9, with estimated statistic and systematic uncertainties of 0.21×10^{-26} J nm^9 and 0.25×10^{-26} J nm^9, respectively. This result, which agrees with previously published semiempirical ones, has been achieved using two more thermodynamical states with respect to [10] and a new method of analysis which takes into account the dependence on the potential contained in all the coefficients of the Q expansion of the direct correlation function $c(Q)$. The adopted method has also allowed a more complete use of the full Q range measured in the experiment, thus exploiting the physical information contained in the data down to 0.5 nm^{-1}. A determination of ν and B independent of any assumption for u_2 could be obtained from the density dependence of the cubic coefficient γ_3 in the low-Q expansion (13) of $c(Q)$. This however requires more accurate data than those presently available.

Acknowledgments

It is a pleasure to acknowledge the assistance of the Laboratoire Léon Brillouin and its staff, particularly Dr J Teixeira in providing the neutron instrument PAXE with its neutron beam and supporting facilities. We thank Dr R A Robinson for his assistance in providing the isotopic Kr sample and Dr E Guarini for useful suggestions during the data analysis. CJB and PAE acknowledge the financial support of the Canadian Natural Sciences and Engineering Research Council, and PV acknowledges the financial support of Università di Firenze, Dipartimento di Fisica.

Appendix

The intensity of neutrons scattered by the cell including the sample, I_{sc}^{exp}, contains contributions from single scattering $I_{sc}^{(1)}$, background scattering B_{sc} and multiple scattering $I_{sc}^{(m)}$:

$$I_{sc}^{exp} = I_{sc}^{(1)*}(\theta) + I_{sc}^{(m)*}(\theta) + B_{sc}(\theta) \tag{A1}$$

where the asterisk denotes that these intensities are attenuated by the sample and by (the sapphire windows of) the cell. Similarly, we have for the empty container:

$$I_{c}^{exp}(\theta) = I_{c}^{(1)*}(\theta) + I_{c}^{(m)*}(\theta) + B_{c}(\theta) \tag{A2}$$

where the asterisk now means attenuation by the cell only. The attenuation is represented by the Paalman–Pings factors $A_{\alpha\beta}$ with α representing the scatterer and β the attenuator:

$$I_{sc}^{(1)*} = A_{s,sc} I_s^{(1)} + A_{c,sc} I_c^{(1)} \tag{A3}$$

and similar expressions for the other attenuated intensities.

The differential cross section at scattering angle θ is related to the fully corrected intensity of neutrons scattered by the sample by:

$$\frac{d\sigma(\theta)}{d\Omega} = \frac{I_s^{(1)}(\theta)}{N\Phi\varepsilon\Delta\Omega} = \frac{I_s^{(1)}(\theta)}{NM(\theta)} \tag{A4}$$

with Φ the incident neutron flux density, N the number of atoms in the sample, ε the (wavelength-dependent) detector efficiency and $\Delta\Omega$ the solid angle in the direction θ. In the present case:

$$A_{s,sc}(0) = t_{sc} = \exp(-\mu_s d_s - \mu_c d_c) = t_s t_c \tag{A5}$$

with t_α the transmission of component α having attenuation coefficient μ_α and thickness d_α.

We measured t_V, t_{CH_4}, t_c and t_{sc} using the direct neutron beam and the cadmium stop to determine backgrounds. When inserting these results in the following formulae (e.g. (A6)), we assume that all neutrons in the beam have a wavelength of 0.4 nm. The effect of the possible presence of faster neutrons, mentioned in section 4, will be considered below. Since the present experiment is restricted to small scattering angles the angular dependence of $A_{\alpha,\beta}(\theta)$ is small, in our case not more than 0.2%, while $A_{s,sc}(\theta) \approx A_{c,sc}(\theta)$.

The multiple scattering $I_s^{(m)}(\theta)$ has been calculated by means of a Monte Carlo simulation using MSCAT [23, 24]. It does not exceed 3% of the single scattering at the highest density.

From the intensities with empty beam I_{eb}, and with cadmium I_{Cd} we obtain the background:

$$\begin{aligned} B_{sc} &= I_{Cd} + t_{sc}(I_{eb} - I_{Cd}) \qquad B_c = I_{Cd} + t_c(I_{eb} - I_{Cd}) \\ B_V &= I_{Cd} + t_V(I_{eb} - I_{Cd}) \end{aligned} \tag{A6}$$

which is to be subtracted from the measured intensities. The single scattering, not yet normalized in absolute units, is then:

$$I_s^{(1)} = \frac{\delta_s}{t_{sc}}[I_{sc}^{exp} - I_{Cd} - t_s(I_c^{exp} - I_{Cd})] \tag{A7}$$

where δ_s is the ratio of single to total scattering as calculated with MSCAT.

For the normalization with vanadium we use for $M(\theta)$ in equation (A4):

$$M_V(\theta) = \frac{I_V^{(1)}}{N_V[1 + P_V(\theta)]\sigma_{inc,V}/4\pi} \tag{A8}$$

where $I_V^{(1)}$ is obtained similarly to (A7) by:

$$I_V^{(1)} = \frac{\delta_V}{t_V}\{I_V^{exp} - I_{Cd} - t_V(I_{eb} - I_{Cd})\} \tag{A9}$$

and P_V is the Placzek correction [18]. For normalization with CH_4 we use a model for $d^2\sigma/d\Omega\, dE$ [25] and obtain $M(\theta)$ by:

$$M_{CH_4}(\theta) = \frac{I_{CH_4}^{(1)}}{N_{CH_4}(d\sigma(\theta)/d\Omega)_{CH_4}} \tag{A10}$$

where $I_{CH_4}^{(1)}$ is obtained similarly to equation (A7) and

$$\left[\frac{d\sigma(\theta)}{d\Omega}\right]_{CH_4} = \frac{1}{\varepsilon(E_0)}\int_{E_{min}}^{E_{max}} \frac{d^2\sigma}{d\Omega\, dE}\varepsilon(E)\, dE \tag{A11}$$

with the integral taken at constant θ and the detector efficiency is given by:

$$\varepsilon(E) = 1 - \exp[-\alpha\lambda(E)]$$

with $\alpha = 1.68\ \mathrm{nm}^{-1}$. It is found that the V-normalized Kr data extrapolate at all densities to an S_0 value about 10% higher than $S(0)$ obtained from *PVT* data. This is the overall accuracy of the absolute normalization using vanadium. However, the CH_4-normalized results agree much better with $S(0)$, and were therefore used for the analysis described in section 5.

If a halo of neutrons with wavelength different from 0.4 nm is present, then it is necessary to re-evaluate the transmission factors appearing in (A6) for the new wavelength. For the case of ^{86}Kr there is only a minor change with wavelength, but for vanadium, methane and the container the change is larger and may be derived from published data. As a test of the significance of this effect, the background correction has been also performed assuming an average halo wavelengths of 0.1 nm. The resulting instrumental normalization factors M_{CH_4} were identical, thus demonstrating the insensitivity of this function to the choice of the halo wavelength. Moreover, using the methane normalization and assuming an average halo wavelength of 0.1 nm, the differences for $c(Q)$ obtained with or without explicit correction for the halo are much smaller than the experimental errors, and, therefore, this correction has not been applied. We remark that in both cases the data normalization procedure was the same.

References

[1] Enderby J E, Gaskell T and March N H 1965 *Proc. Phys. Soc.* **85** 217
[2] Casanova G, Dulla R J, Jonah D A, Rowlinson J S and Saville G 1970 *Mol. Phys.* **18** 589
[3] Axilrod R M and Teller E 1943 *J. Chem. Phys.* **11** 299
[4] Matthai C C and March N H 1982 *Phys. Chem. Liquids* **11** 207
[5] Reatto L and Tau M 1992 *J. Phys.: Condens. Matter* **4** 1
[6] Magli R, Barocchi F, Chieux P and Fontana R 1996 *Phys. Rev. Lett.* **77** 846
[7] Teitsma A and Egelstaff P A 1980 *Phys. Rev.* A **21** 367
[8] Barocchi F, Zoppi M and Egelstaff P A 1985 *Phys. Rev.* A **31** 2732
[9] Tau M, Reatto L, Magli R, Egelstaff P A and Barocchi F 1989 *J. Phys.: Condens. Matter* **1** 7131
[10] Formisano F, Benmore C J, Bafile U, Barocchi F, Egelstaff P A, Magli R and Verkerk P 1997 *Phys. Rev. Lett.* **79** 221
Benmore C J, Formisano F, Magli R, Bafile U, Barocchi F, Egelstaff P A, Robinson R A and Verkerk P 1997 *Physica* B **234–236** 313
[11] Terburg B P, Verkerk P, Jericha E and Zawisky M 1993 *Nucl. Instrum. Methods Phys. Res.* A **324** 247
[12] Sears V F 1992 *Neutron News* **3** 26
[13] Jůza J and Šifner O 1976 *Acta Tech. ČSAV* **1** 1
[14] Benmore C J, Mos B, Verkerk P and Egelstaff P A 1998 *J. Neutron Res.* **6** 279
[15] Nieman H F, Tennant D C and Dolling G 1980 *Rev. Sci. Instrum.* **51** 1299
[16] Teixeira J 1996 private communication
[17] Egelstaff P A 1987 *Neutron Scattering* part B, ed D L Price and K Sköld (San Diego: Academic) p 405
[18] Yarnell J L, Katz M J, Wenzel R G and Koenig S H 1973 *Phys. Rev.* A **7** 2130
[19] Standard J M and Certain P R 1985 *J. Chem. Phys.* **83** 3002
[20] Kumar A and Meath W J 1985 *Mol. Phys.* **54** 823
[21] Leonard P J and Barker J A 1975 *Theor. Chem. Adv. Perspect.* **1** 117
[22] Aziz R A and Slaman M J 1986 *Mol. Phys.* **58** 679
In a more recent paper (Dham A K, Allnatt A R, Meath W J and Aziz R A 1989 *Mol. Phys.* **67** 1291) a new HFD-B type potential for Kr has been proposed. The calculated $c_0(Q)$ and $c_1(Q)$ differ from those obtained with the AS potential by an amount much smaller than our experimental uncertainties.
[23] Copley J R D 1974 *Comput. Phys. Commun.* **7** 289
Copley J R D 1975 *Comput. Phys. Commun.* **9** 59
[24] Copley J R D, Verkerk P, van Well A A and Fredrikze H 1986 *Comput. Phys. Commun.* **40** 337
[25] Griffing G 1961 *Phys. Rev.* **124** 1489